

Non-hydrostatic effects in layered shallow water flows

By DAVID Z. ZHU[†] AND GREGORY A. LAWRENCE

Department of Civil Engineering, University of British Columbia,
Vancouver, BC, V6T 1Z4, Canada
e-mail: zhu@civil.ubc.ca; lawrence@civil.ubc.ca

(Received 9 October 1996 and in revised form 29 August 1997)

This paper develops a one-dimensional extension to classical layered hydraulics that incorporates non-hydrostatic effects. General results for a homogeneous layer in a multi-layer steady flow are applied to single- and two-layer flow over a two-dimensional sill. The equation obtained for single-layer flows is the same as that obtained by Naghdi & Vongsarnpigoon (1986) using the direct theory of constrained fluid sheets, and compares very well with the laboratory measurements of Sivakumaran *et al.* (1983). The new equation derived for two-layer flows provides excellent agreement with the laboratory measurements of Lawrence (1993). Accurate solutions are obtained for a regime of two-layer flow whose behaviour cannot be explained, even qualitatively, using classical hydraulic theory.

1. Introduction

This paper considers multi-layered shallow water flows over two-dimensional obstacles in a channel of constant width. Such flows are usually modelled as homogeneous layers of inviscid fluid with negligibly small vertical velocities. Consequently, the pressure distribution can be considered hydrostatic and the horizontal velocity uniform with depth in each layer. The resulting equations, called the hydraulic (or shallow water) equations, are used extensively in the study of single-layer flows, see, for example, Henderson (1966). The extension of the hydraulic equations to two-layer flows is known as internal hydraulic theory. Internal hydraulic theory is widely used to study various two-layer flow problems, including flow over a broad-crested weir (Wood & Lai 1972), flow over a sill (Long 1974; Baines 1984, 1988; Lawrence 1993), flow through a contraction (Armi & Farmer 1986; Lawrence 1990; Helfrich 1995), and flow through the combination of a contraction and a sill (Armi 1986; Farmer & Armi 1986; Dalziel 1991).

The hydraulic approach is generally valid when the streamline curvature is small. However, the effects of streamline curvature and non-hydrostatic pressure cannot always be ignored. The primary motivation for the present study was the desire to model a regime of two-layer flow, called Approach-controlled flow, where hydraulic theory fails owing to the neglect of streamline curvature (Lawrence 1993). In Approach-controlled flow an internal hydraulic control is located near the foot of the obstacle (the exact location is weakly dependent on friction forces). Between the point of control and the crest of the obstacle the interface rises approximately in accordance

[†] Present address: Department of Civil and Environmental Engineering, University of Alberta, Edmonton, Alberta, T6G 2G7, Canada. e-mail: dzhu@civil.ualberta.ca.

with hydraulic theory. Downstream of the crest the interface level drops rapidly, and the flow changes from a supercritical flow in which the upper layer is thinner, to one in which the lower layer is thinner. This transition (called the ‘supercritical leap’ by Lawrence 1993 and Baines 1995) involves significant streamline curvatures and is not predicted by hydraulic theory.

Although Approach-controlled flows display unusual behaviour they are by no means uncommon. Lawrence (1993) shows that these flows often occur over a wider range of parameters than either Crest-controlled or Subcritical flows, and that field observations of Approach-controlled flows are presented in Farmer & Denton (1985, figure 4) and Murray, Hecht & Babcock (1983, figure 10).

Several studies have addressed the effects of streamline curvature in layered flows. Dressler (1978), Sivakumaran, Hosking & Tingsanchali (1981) and Sivakumaran, Tingsanchali & Hosking (1983) studied single-layer flow over curved beds by transforming the equations of motion using orthogonal curvilinear coordinates. Naghdi & Vongsarnpigoon (1986) have used the direct theory of constrained fluid sheets to accurately describe single-layer flows. Pratt (1984) studied single-layer flow over adjacent small obstacles. Melville & Helfrich (1987), Shen, Shen & Sun (1989) and Shen (1992) have used extensions of the Korteweg–de Vries equation to study transcritical ($F^2 \approx 1$) flow over small sills with small disturbances to the free surface (in single-layer flow), or to the interface (in two-layer flow). Khan & Steffler (1996) studied single-layer flow over curved beds using vertically averaged and moment equations. Finally, fully nonlinear solutions using conformal mapping techniques have been successfully applied to a wide range of single- and two-layer flows (King & Bloor 1990; Belward & Forbes 1993; Zhang & Zhu 1996). Our objective is to develop a one-dimensional extension to classical layered hydraulics that will help clarify the importance of non-hydrostatic effects, particularly in Approach-controlled flows. To achieve this objective we have chosen to extend the approach of Pratt (1984) to examine two-layer flow over a sill of finite height.

In §2 we present a general extension of hydraulic theory to incorporate non-hydrostatic effects in multi-layered flows. In §3 the equations for single-layer flow over a bottom sill are derived and then compared with the theoretical results of Naghdi & Vongsarnpigoon (1986), and the experimental results of Sivakumaran *et al.* (1983). In §4 the equations for two-layer flow over a bottom sill are derived and then compared with the experimental measurements of Lawrence (1993). Our conclusions are stated in §5.

2. Equation derivation

We study a homogenous layer within a multi-layered steady flow over a two-dimensional sill in a channel of constant width, see figure 1. The fluid is assumed to be inviscid and incompressible, and the flow irrotational. The density is constant within each layer, but increases for each successively deeper layer. We ignore regions of flow where there are significant energy losses, e.g. internal hydraulic jumps and regions of flow separation.

Following Pratt (1984), we use the length of the sill, L , and the upstream depth of flow, H , as the horizontal and vertical length scales. Unlike Pratt (1984), we allow the obstacle to be of finite height, i.e. $\beta_m = \beta_m^*/H = O(1)$. (Note that we use an asterisk to distinguish dimensional from non-dimensional variables). Following Long (1954) we require that the obstacle be of ‘easy’ shape with its minimum radius of curvature, $R \gg H$. Given that $R = O(L^2/H)$, we introduce the small parameter $\sigma = O(H/L)^2 \ll 1$.

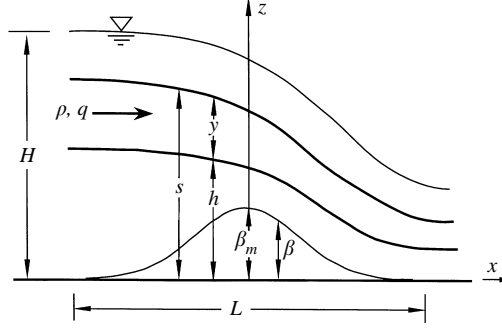


FIGURE 1. Schematic of multi-layer flow over a sill.

Taking $(gH)^{1/2}$ and $(\sigma gH)^{1/2}$ as the horizontal and vertical velocity scales, and ρgH as the pressure scale, we obtain the following set of dimensionless variables of $O(1)$:

$$x = \frac{x^*}{L}, \quad z = \frac{z^*}{H}, \quad q = \frac{q^*}{(gH^3)^{1/2}}, \quad u = \frac{u^*}{(gH)^{1/2}}, \quad w = \frac{w^*}{(\sigma gH)^{1/2}}, \quad P = \frac{P^*}{\rho gH}, \quad (1)$$

where ρ is the density (assumed constant within each layer), u and w are the horizontal and vertical velocities, P is the pressure, and q is the two-dimensional flow rate.

Using (1), we obtain the following dimensionless equations and boundary conditions governing the flow in each layer:

$$\text{the momentum equations} \quad uu_x + wu_z = -P_x, \quad (2a)$$

$$\sigma(uw_x + ww_z) = -P_z - 1, \quad (2b)$$

$$\text{the continuity equation} \quad u_x + w_z = 0, \quad (2c)$$

$$\text{the irrotationality condition} \quad u_z - \sigma w_x = 0, \quad (2d)$$

and the boundary conditions

$$P = P_s \quad \text{and} \quad w = us_x \quad \text{at} \quad z = s, \quad (2e, f)$$

$$\text{and} \quad w = uh_x \quad \text{at} \quad z = h, \quad (2g)$$

where P_s is the pressure at the top of the layer, $z = s(x)$ and $z = h(x)$ are the elevations of the top and the bottom of the layer respectively, and $s = y + h$, with y being the layer thickness. Differentiation with respect to x and z is denoted by subscripts.

Integrating (2a) and (2b) with respect to x and z , and applying (2d), yields

$$E \equiv P + \rho gz + \frac{1}{2}\rho(u^2 + w^2), \quad (2h)$$

where E is the Bernoulli constant (mechanical energy per unit volume), and is constant throughout the layer. It is customary to simplify (2h) by neglecting the vertical velocity and assuming a hydrostatic pressure distribution. However, in the present study, we will include the non-hydrostatic pressure and the vertical velocity.

Expanding u , w , P and E in terms of the small parameter σ :

$$u = u_0 + \sigma u_1 + \dots, \quad w = w_0 + \sigma w_1 + \dots, \quad (3a, b)$$

$$P = P_0 + \sigma P_1 + \dots, \quad E = E_0 + \sigma E_1 + \dots, \quad (3c, d)$$

and substituting (3) into (2) yields, to zeroth order,

$$u_0 u_{0x} + w_0 u_{0z} = -P_{0x}, \quad (4a)$$

$$0 = -P_{0z} - 1, \quad (4b)$$

$$u_{0x} + w_{0z} = 0, \quad (4c)$$

$$u_{0z} = 0, \quad (4d)$$

$$P_0 = P_s \quad \text{and} \quad w_0 = u_0 s_x \quad \text{at} \quad z = s, \quad (4e, f)$$

and

$$w_0 = u_0 h_x \quad \text{at} \quad z = h. \quad (4g)$$

Pratt (1984) treated the case where $\beta_m = O(\sigma^2)$ which yields $w_0 = 0$, whereas we allow $\beta_m = O(1)$ and $w_0 \neq 0$. From (4d), u_0 is a function of x only. Integrating (4c) vertically and applying (4f) and (4g), yields

$$u_0 = U = q/y, \quad (5)$$

and

$$w_0 = U \left\{ \left(\frac{z-h}{y} \right) y_x + h_x \right\}. \quad (6)$$

Integrating (4b) vertically from z to s and applying (4e), the pressure, to zeroth order, is hydrostatic, i.e.

$$P_0 = P_s + s - z. \quad (7)$$

Integrating (4a) with respect to x , and applying (4d) and (7), yields

$$E_0 = P_s + y + h + \frac{1}{2}U^2, \quad (8)$$

which is the result used in classical hydraulic theory.

To first order, (2) becomes

$$u_0 u_{1x} + u_1 u_{0x} + w_0 u_{1z} + w_1 u_{0z} = -P_{1x}, \quad (9a)$$

$$u_0 w_{0x} + w_0 w_{0z} = -P_{1z}, \quad (9b)$$

$$u_{1x} + w_{1z} = 0, \quad (9c)$$

$$u_{1z} - w_{0x} = 0, \quad (9d)$$

$$P_1 = 0 \quad \text{and} \quad w_1 = u_1 s_x \quad \text{at} \quad z = s, \quad (9e, f)$$

and

$$w_1 = u_1 h_x \quad \text{at} \quad z = h. \quad (9g)$$

Using (6), u_1 can be obtained by integrating (9d) vertically:

$$u_1 = U \left\{ \frac{(z-h)^2}{2y^2} (-2y_x^2 + yy_{xx}) + \frac{z}{y} (-2y_x h_x + y h_{xx}) \right\} + c(x). \quad (10)$$

Integrating (3a) vertically from h to s , and using $u_0 = U$, yields

$$\int_h^s u_1 dz = O(\sigma). \quad (11)$$

Integrating (10) vertically from h to s and applying (11), we obtain

$$u_1 = U \left\{ \frac{3(z-h)^2 - y^2}{6y^2} (-2y_x^2 + yy_{xx}) + \frac{2(z-h) - y}{2y} (-2y_x h_x + y h_{xx}) \right\}. \quad (12)$$

Integrating (9b) vertically from z to s , after applying (9d), (9e) and (4d), yields

$$P_1 = u_{0s} u_{1s} + \frac{1}{2} w_{0s}^2 - u_0 u_1 - \frac{1}{2} w_0^2, \quad (13)$$

where the subscript s indicates that the parameter is evaluated at the top of the layer.

Integrating (9a) with respect to x , and using (9d) and (4d), yields

$$E_1 = u_{0s} u_{1s} + \frac{1}{2} w_{0s}^2. \quad (14)$$

Both P_1 and E_1 are dependent on the vertical velocity as well as vertical variations of the horizontal velocity. Substituting w_0 and u_1 into (13), and u_0 , u_1 and w_0 into (14), the first-order corrections to the pressure and the energy become

$$P_1 = U^2 \left\{ \frac{y^2 - (z-h)^2}{2y^2} (y y_{xx} - y_x^2) + \frac{y - (z-h)}{y} (y h_{xx} - h_x y_x) \right\}, \quad (15)$$

$$E_1 = U^2 \{ y(2y_{xx} + 3h_{xx}) - y_x^2 + 3h_x^2 \} / 6. \quad (16)$$

The vertical velocity w_1 can also be obtained using (9c), (9f) and (9g), but is not needed in the present study.

Thus to $O(\sigma^2)$, the Bernoulli constant (layer energy) can be expressed as

$$E = P_s + y + h + \frac{1}{2} U^2 + \frac{1}{6} \sigma U^2 \{ y(2y_{xx} + 3h_{xx}) - y_x^2 + 3h_x^2 \}, \quad (17)$$

and the pressure on the bottom of the layer P_h as

$$P_h = P_s + y + \frac{1}{2} \sigma U^2 \{ y(y_{xx} + 2h_{xx}) - y_x^2 - 2y_x h_x \}. \quad (18)$$

In multi-layer flow problems, the pressure is continuous at layer interfaces, and the layer energy is conserved within each of the layers. The combination of (17) and (18) can be used to solve problems with any number of layers. The above equations will be used to study curvature effects in both single- and two-layer flows.

3. Curvature effects in single-layer flows

We now study single-layer flows over a smooth sill with $\sigma \ll 1$ in a channel of constant width. Setting the pressure at the free surface $P_s = 0$, the layer energy and the pressure on the bed can be obtained from (17) and (18). To $O(\sigma^2)$ the energy can be expressed as

$$E = E_0 + \sigma E_1, \quad (19a)$$

where

$$E_0 = y + \beta + \frac{1}{2} U^2, \quad (19b)$$

and

$$E_1 = U^2 \{ y(2y_{xx} + 3\beta_{xx}) - y_x^2 + 3\beta_x^2 \} / 6. \quad (19c)$$

To $O(\sigma^2)$ the pressure on the bed can be expressed as:

$$P = P_0 + \sigma P_1, \quad (19d)$$

where

$$P_0 = y, \quad (19e)$$

and

$$P_1 = \frac{1}{2} U^2 \{ y(y_{xx} + 2\beta_{xx}) - y_x^2 - 2y_x \beta_x \}. \quad (19f)$$

E_0 and P_0 are the zeroth-order (hydrostatic) components, and E_1 and P_1 are the first-order modifications due to the curvature effects. Naghdi & Vongsarnpigoon (1986) obtained (19c) using the direct theory of constrained fluid sheets. However, we have not used this method since it is not readily applicable to two-layer flows (Naghdi, personal communication).

After differentiating (19a) with respect to x and using (19b), we can write to $O(\sigma^2)$,

$$\frac{dy}{dx} = -\frac{S_0 + S_c}{1 - F^2} \quad (20a)$$

where the topographic slope for a straight channel

$$S_0 = \sigma^{1/2}(F^2\beta_x), \quad (20b)$$

and the slope due to the curvature effects

$$S_c = \sigma dE_1/dx, \quad (20c)$$

with $F^2 = U^2/y$ being the Froude number. Equation 20(a) requires that $S_0 + S_c = 0$ at the critical point ($F^2 = 1$). For hydrostatic crest-controlled flow, the flow is critical at $S_0 = 0$, which is satisfied at the crest of the sill. However, when the curvature effects are included, the critical point is shifted to the position where $S_0 + S_c = 0$.

Equation (19) is a nonlinear second-order ordinary differential equation that can be arranged in the following form:

$$\sigma y_{xx} - \frac{1}{2}\sigma y^{-1}y_x^2 + a_1 y^{-1} + a_2 y + a_3 y^2 + \frac{3}{2}\sigma\beta_{xx} = 0, \quad (21)$$

where $\sigma \ll 1$, and

$$a_1 = \frac{3}{2}(1 + \sigma\beta_x^2), \quad a_2 = -3(E - \beta)q^{-2}, \quad a_3 = 3q^{-2},$$

where a_1 , a_2 and a_3 are of $O(1)$. The energy E cannot be prescribed in advance and must be obtained using the conditions at the critical point.

Given that the coefficient in the y_{xx} term in (21) is small (i.e. $\sigma \ll 1$), we have a stiff nonlinear second-order ordinary differential equation. Such an equation presents a mathematical challenge, see for example, Ascher, Mattheij & Russell (1995). The problem is further complicated by the fact that the location of the critical point, i.e. the point of transition from subcritical to supercritical flow, now depends on the solution and is not known in advance, see (20a). Numerical instabilities prevented Naghdi & Vongsarnpigoon (1986) from solving (21) using a shooting method.

We have successfully solved (21) as a boundary value problem using COLNEW, a general-purpose code for solving mixed-order systems of boundary-value problems in ordinary differential equations, developed by Ascher, Christiansen & Russell (1981). In applying the code, two boundary conditions are needed. With the constant-energy equation, the flow conditions at the two boundaries are related. The equation is then solved using trial and error by adjusting one boundary condition until the control condition is satisfied.

Equation (21) can also be solved by iteration starting from the hydrostatic solution. For single-layer flows, hydrostatic solutions provide a good starting point. However, this method is not applicable when the hydrostatic solution does not even predict the correct regime of flow, such as in two-layer Approach-controlled flows (discussed in §4).

3.1. Comparison with experimental results

Sivakumaran *et al.* (1983) studied single-layer flow over a Gaussian sill satisfying $\beta = \beta_m \exp[-4x^2]$, with $\beta_m = 0.58$, $q = 0.178$, and $\sigma = 0.032$. Their measurements are compared with predictions made using both hydrostatic theory and the extended non-

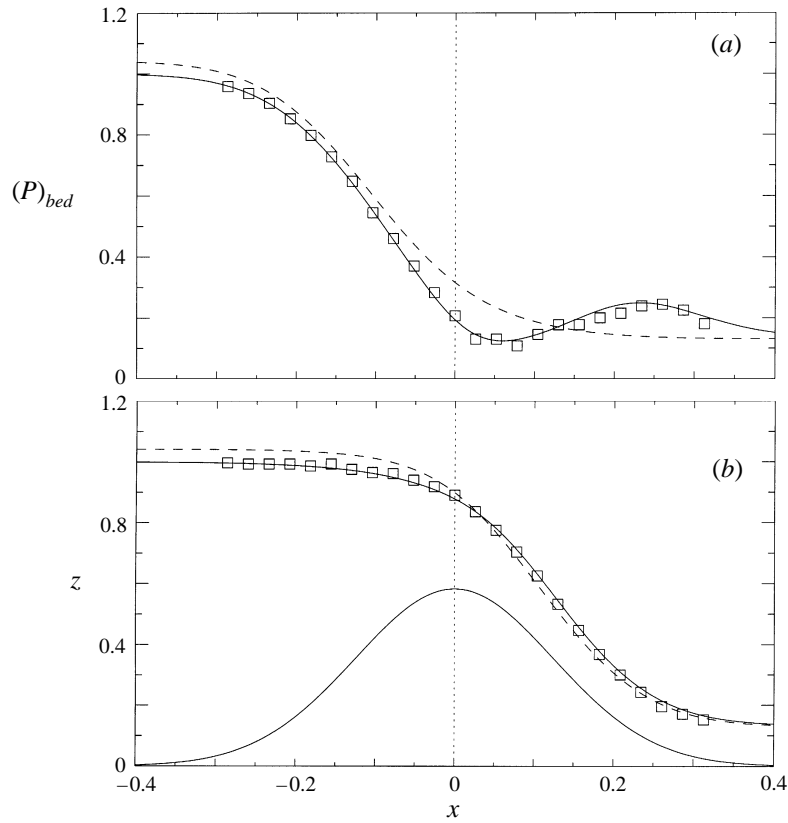


FIGURE 2. Comparison of the predicted and measured: (a) pressure on the bed, and (b) surface elevation, for the laboratory experiment of Sivakumaran *et al.* (1983), with $\beta = \beta_m \exp[-4x^2]$, $\beta_m = 0.58$, $q = 0.178$, and $\sigma = 0.032$. —, Predictions of the extended theory; - - - - - , hydrostatic predictions; \square , measurements.

hydrostatic theory in figure 2. The extended theory provides much better predictions of the pressure on the bed and of the depth of flow. The hydrostatic theory predicts a monotonic decrease in pressure as the flow passes over the obstacle. However, the measurements of Sivakumaran *et al.* (1983) show that the pressure reaches a minimum just downstream of the crest, then rises to a peak halfway down the lee side of the sill. The non-hydrostatic theory matches these measurements extremely well. To explain the differences between the hydrostatic and non-hydrostatic predictions we begin by considering the non-hydrostatic corrections to the pressure on the bed, $(P_1)_{bed}$, and to the energy, E_1 .

The expression for the non-hydrostatic pressure, (19f), consists of terms due to the streamline curvature, i.e. terms containing the second derivatives (β_{xx} and y_{xx}), and terms due to the slope of the streamlines, i.e. terms containing the first derivatives (y_x and β_x). However, we see from figure 3(a) that P_1 is mainly caused by streamline curvature. At the crest of the obstacle the flow is concave downward yielding an upward centrifugal force and, as we would expect, a negative value for P_1 . Similarly P_1 is positive at locations where the flow is concave upward. Note that, even though the sill has maximum curvature at the crest, the minimum value of P_1 occurs just downstream of the crest. This occurs because centrifugal forces are proportional to the velocity squared, and the velocity increases as the flow passes over the crest.

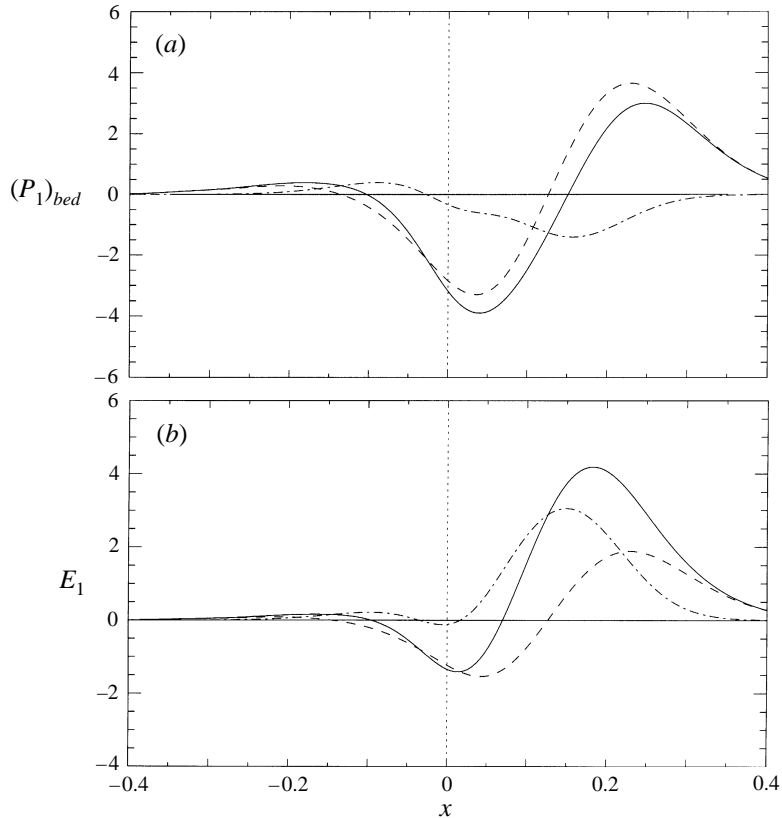


FIGURE 3. The non-hydrostatic component of (a) pressure and (b) internal energy for the experiment of Sivakumaran *et al.* (1983). The total non-hydrostatic component (—) has been separated into the non-hydrostatic component due to streamline curvature (----), and that due to the slope of the streamlines (-·-·-·-).

The non-hydrostatic component of energy, E_1 , exhibits the same general variation as P_1 , see figure 3(b). Immediately upstream of the crest $dE_1/dx < 0$, so from (20c) $S_c < 0$; whereas, from (20b) $S_0 > 0$. Therefore, the critical point ($x = x_c$), where $F = 1$ and $S_0 + S_c = 0$, occurs just upstream of the crest. From figure 4(a) we see that this point is located at $x_c \approx -0.014$. We have also plotted the variation of E_0^{NH} , computed using non-hydrostatic theory, together with the constant E_0^H from hydrostatic theory, see figure 4(b).

At a given location differentiating (19b) with respect to y yields

$$\frac{\partial E_0}{\partial y} = 1 - F^2, \quad (22)$$

and the minimum value of E_0 occurs when $F = 1$. Therefore, $E_0^{NH} < E_0^H$ at $x = x_c$, because $F = 1$ in the non-hydrostatic solution, but $F < 1$ in the hydrostatic solution. Given that E_1 is negative at the critical point, then $E_0^{NH} < E_0^H$ is also true upstream of the obstacle. This result means that the non-hydrostatic predictions for the depth of flow (and, consequently, the pressure on the bed) upstream of the obstacle are less than the hydrostatic predictions, as shown in figure 2. Thus an important effect of the centrifugal forces present as flow passes over an obstacle is a reduction in the upstream

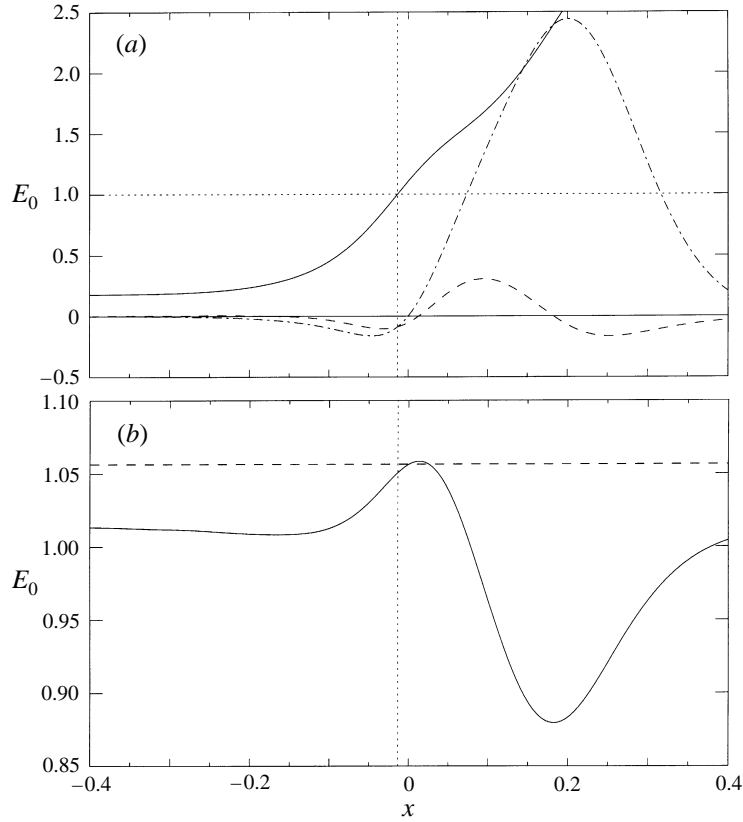


FIGURE 4. Predictions of the extended theory for the experiment of Sivakumaran *et al.* (1983). (a) —, F ; ---, S_c ; -·-·-, $(-S_0)$; (b) —, E_0^{NH} ; ---, E_0^H . The vertical dotted lines are drawn at the critical point $x = x_c \approx -0.014$, where $F = 1$ and $S_c = -S_0$.

depth required to pass a given flow rate over the obstacle. This result will hold true as the curvature of the obstacle increases, providing the flow does not separate on the lee side of the sill.

4. Curvature effects in two-layer flows

We study two-layer flows over a two-dimensional smooth sill in a channel of constant width (figure 5). The flow is assumed to be shallow with $\sigma = (H/L)^2 \ll 1$, where H and L are the upstream depth and the sill length, respectively. We make the assumption that the density difference between the upper and lower layers is smaller than the shallowness parameter, i.e. $\epsilon = (\rho_l - \rho_u)/\rho_l \ll \sigma$, (the subscripts u and l refer to the upper and lower layer, respectively), in which case, we can assume that the free surface is horizontal. Normalizing with respect to H , L , ρ_l , g , and $g' = \epsilon g$, yields

$$\left. \begin{aligned} x &= \frac{x^*}{L}, & z &= \frac{z^*}{H}, & y_u &= \frac{y_u^*}{H}, & y_l &= \frac{y_l^*}{H}, & q_u &= \frac{q_u^*}{(g'H^3)^{1/2}}, \\ q_l &= \frac{q_l^*}{(g'H^3)^{1/2}}, & P_u &= \frac{P_u^*}{\rho_l gH}, & P_l &= \frac{P_l^*}{\rho_l gH}, & E_u &= \frac{E_u^*}{\rho_l gH}, & E_l &= \frac{E_l^*}{\rho_l gH}. \end{aligned} \right\} \quad (23)$$

The asterisks indicate dimensional variables. All the dimensionless variables are of

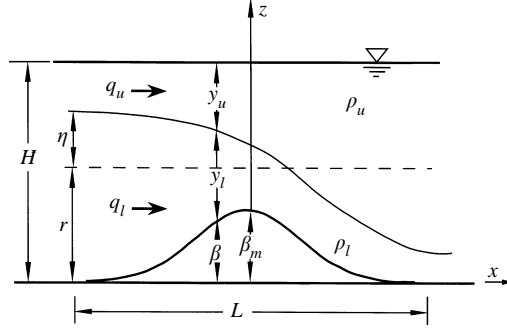


FIGURE 5. Schematic of two-layer flow over a sill.

$O(1)$. We also define the total flow rate, $q = q_u + q_l$, and the flow rate ratio, $r = q_l/q$. In many flows the obstacle does not change the interface height upstream and downstream of it. In such flows the ‘undisturbed’ interface height, y_0 , is determined by external forcing. Following Baines (1984) and Lawrence (1993) we assume barotropic forcing, so that in undisturbed flows the velocity in each layer is equal, and $y_0 = r$. Interface deflections are measured relative to the undisturbed flow, i.e.

$$\eta = y_l + \beta - r, \quad (24)$$

where β is the elevation of the sill, see figure 5.

Given the pressure at the free surface $P_s = 0$, the pressure on the interface and the layer energy for the upper layer can be obtained by replacing U^2 by ϵU^2 in (17) and (18):

$$P_u(x, \eta) = (1 - \epsilon)y_u + \epsilon\sigma\frac{1}{2}U_u^2\{y_u\eta_{xx} + \eta_x^2\}, \quad (25a)$$

$$\text{and} \quad E_u = (1 - \epsilon) + \epsilon(\frac{1}{2}U_u^2) + \epsilon\sigma\frac{1}{6}U_u^2\{y_u\eta_{xx} + 2\eta_x^2\}, \quad (25b)$$

where $U_u = q_u/y_u$ is the mean velocity of the upper layer.

Given that the pressure is continuous across the interface,

$$P_l(x, \eta) = P_u(x, \eta), \quad (26)$$

and using (17), we have for the lower layer

$$E_l = (1 - \epsilon) + \epsilon(\eta + r + \frac{1}{2}U_l^2) + \epsilon\sigma\frac{1}{6}U_l^2[y_l(2\eta_{xx} + \beta_{xx}) - \eta_x^2 + 2\eta_x\beta_x + 2\beta_x^2] + \frac{1}{2}U_u^2[y_u\eta_{xx} + \eta_x^2], \quad (27)$$

where $U_l = q_l/y_l$.

We eliminate the $(1 - \epsilon)$ term by subtracting (25b) from (27), leaving only terms of $O(\epsilon)$. By dividing by ϵ , we then obtain the internal energy for two-layer flows, E , as

$$E = \frac{E_l - E_u}{\epsilon} - r. \quad (28)$$

This internal energy E describes the internal hydraulics of two-layer flows (Lawrence 1993; Zhu 1996). We can write E as the sum of the zeroth-order (hydrostatic) E_0 and the first-order modification due to the flow streamline curvature E_1 :

$$E = E_0 + \sigma E_1, \quad (29a)$$

$$\text{with} \quad E_0 = \eta + \frac{1}{2}(U_l^2 - U_u^2), \quad (29b)$$

$$\text{and} \quad E_1 = \frac{1}{6}U_l^2[y_l(2\eta_{xx} + \beta_{xx}) - \eta_x^2 + 2\eta_x\beta_x + 2\beta_x^2] + \frac{1}{6}U_u^2[2y_u\eta_{xx} + \eta_x^2]. \quad (29c)$$

Given that to $O(\sigma^2)$ E_u and E_l are conserved, E is also conserved throughout the channel in the absence of hydraulic jumps or flow separation. Differentiating (29a) with respect to x and using (29b), the slope of the interface η becomes

$$\frac{d\eta}{dx} = -\frac{S_0 + S_c}{1 - G^2}, \quad (30a)$$

where the topographic slope $S_0 = \sigma^{1/2} F_l^2 \beta_x$, (30b)

and the slope due to flow curvature $S_c = \sigma dE_l/dx$. (30c)

For $\epsilon \ll 1$, the composite Froude number, $G = (F_u^2 + F_l^2)^{1/2}$, where $F_u^2 = U_u^2/y_u$ and $F_l^2 = U_l^2/y_l$ are the densimetric Froude numbers for the upper and lower layer, respectively. Comparing (30) with (20) we see that the composite Froude number, G , serves the same role for two-layer flows, as the classical Froude number, F , does for single-layer (open channel) flows. The locations where $G = 1$ are critical points, and the flow is supercritical (or subcritical) when $G > 1$ (or $G < 1$). At critical points, $S_0 + S_c = 0$ must be satisfied. The exact location of the critical point depends on the flow conditions.

Rearranging (29) we obtain an equation for the interface position η . This equation is a stiff nonlinear second-order ordinary differential equation, similar to (21). Unlike single-layer flows over a sill, some two-layer flows (e.g. Approach-controlled flows) have no hydrostatic solutions, see Lawrence (1993). Thus the iteration method starting from the hydrostatic solution cannot be applied. The equation can be solved numerically as a boundary value problem using the solver COLNEW, as discussed in previous section for single-layer flows.

4.1. Comparison of hydrostatic and non-hydrostatic solutions

We will now compare the ability of hydrostatic and non-hydrostatic theories to predict the behaviour of uni-directional flow over a sill. Baines (1984) and Lawrence (1993) identified four regimes of two-layer uni-directional flows over a sill: Subcritical, Crest-controlled, Supercritical, and Approach-controlled. The first three regimes have their single-layer counterparts, but Approach-controlled flow does not. Following Baines (1984) and Lawrence (1993) we assume barotropic forcing, i.e. if the flow is undisturbed by the presence of the obstacle then both layers move horizontally with the same speed. In this case the regime of flow depends on three parameters: the flow rate ratio, $r = q_l/q$; the non-dimensional obstacle height; $\beta_m = \beta_m/H$; and the undisturbed composite Froude number, $G_0 = q/(r(1-r))^{1/2}$, see Lawrence (1993). For each value of r , classification diagrams can be constructed that predict the values of G_0 and β_m corresponding to each flow regime.

The classification diagram for $r = 0.5$ is plotted in figure 6, together with diagrams showing the variation in interface height for each of the four regimes. For the Subcritical, Crest-controlled, and Supercritical flow regimes the interface variation predicted using hydraulic theory is qualitatively correct. However, in Approach-controlled flows hydrostatic theory provides a poor prediction of the variation in interface height downstream of the crest of the obstacle. Downstream of the crest the interface level drops rapidly, and the flow changes from a supercritical flow in which the upper layer is thinner to one in which the lower layer is thinner. This transition has become known as the ‘supercritical leap’ (Lawrence 1993; Baines 1995).

Our non-hydrostatic extension to hydraulic theory is of significant value if it can effectively model supercritical leaps. To test this ability we have solved equation (29)

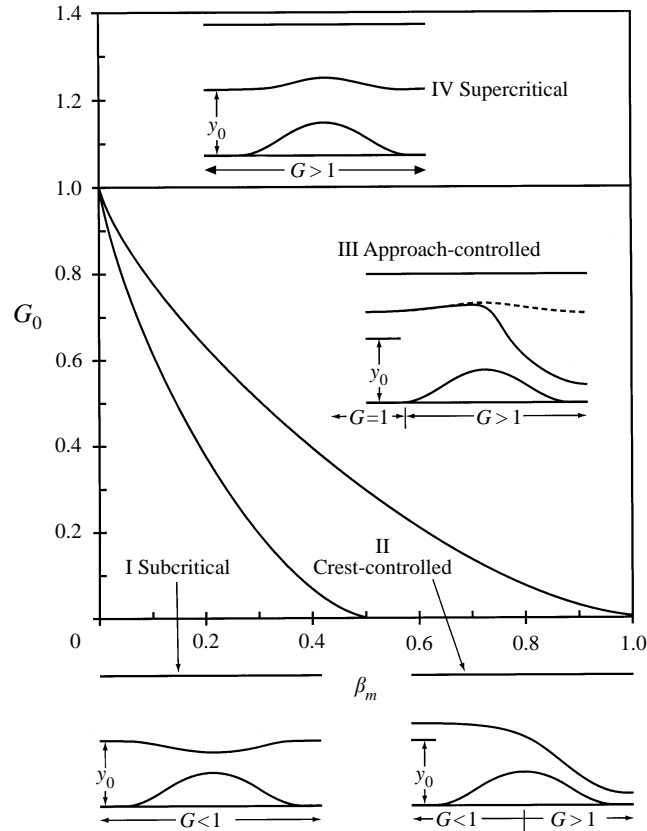


FIGURE 6. Classification diagram for $r = 0.5$ showing the regions of the (β_m, G_0) -plane corresponding to each of the flow regimes (adapted from Lawrence 1993). The dashed line in the sketch of Approach-controlled flow represents the hydrostatic solution.

for the Approach-controlled flow presented as experiment 17 in Lawrence (1993). In this flow, $r = 0.5$, $\beta_m = 0.37$, $G_0 = 0.55$, and $\epsilon = 0.008$. The shape of the obstacle is given by $\beta = \beta_m \cos^2(\pi x)$ (for $|x| \leq 0.5$), and $\sigma = 0.046$. The non-hydrostatic predictions closely match the supercritical leap observed in the laboratory experiments, see figure 7(a). The discrepancies between the predicted and measured interface levels are of order 1 cm. Such discrepancies may be a result of the shear-induced interfacial mixing which makes it difficult to determine the exact location of the interface, see Lawrence (1993, figure 6c). The prediction of the hydrostatic theory is also shown in figure 7(a). It is clear that the hydrostatic theory fails to predict the supercritical leap.

As the flow passes through the supercritical leap at $0.1 < x < 0.2$, it changes from having a thinner upper layer ($G \approx F_u$) to having a thinner lower layer ($G \approx F_l$). During the transition the composite Froude number initially drops as both layers become comparable in thickness, and then increases dramatically as the lower layer thins. This transition is not modelled by hydrostatic theory since the flow is far from hydrostatic in the vicinity of $x = 0.15$. At $x \approx 0.15$ the combination of high streamline curvature and high lower-layer velocity results in a large negative value of E_1 (figure 7c). It is interesting to note that the composite Froude number drops to unity (see figure 7b) at $x \approx 0.15$. This should not be interpreted to mean that there is an internal hydraulic control at $x \approx 0.15$. The result that $G^2 = 1$ at positions of control is based on the assumption that the flow is hydrostatic.

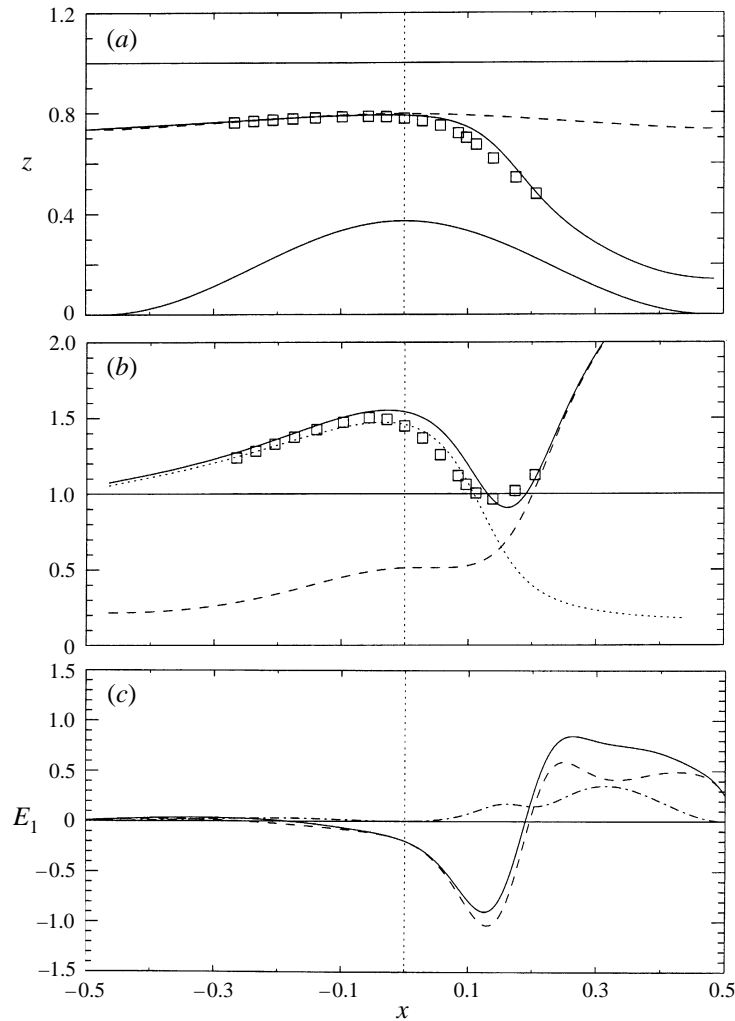


FIGURE 7. Comparison of the predictions of the extended theory with experiment 17 of Lawrence (1993). (a) Interface position: —, prediction of the extended theory; ----, hydrostatic prediction; \square , measurements. (b) —, Prediction of G ; $\cdots\cdots$, F_1 ; ----, F_2 , using the extended theory. \square , measurements of G . (c) —, Total non-hydrostatic energy E_1 ; ----, non-hydrostatic energy due to streamline curvature; -·-·-, non-hydrostatic energy due to streamline slope.

To obtain a more extensive comparison between the hydrostatic and non-hydrostatic predictions we set $r = 0.5$, and $\beta_m = 0.37$ (as in experiment 17 of Lawrence 1993), but rather than fixing $G_0 = 2q = 0.55$, we allow G_0 to vary between 0 and 1.2. By doing so we model changes to the flow with increasing flow rate while all the other flow parameters are held constant. Figure 8 presents the changes in the predicted composite internal Froude number at the crest, G_c , and at the upstream and downstream ends of the obstacle, G_u and G_d , respectively. For the purpose of comparing the hydrostatic and non-hydrostatic solutions we have ignored the possibility of jumps forming over the lee face of the obstacle. In Crest- and Approach-controlled flows an internal hydraulic jump will form either over the lee face of the obstacle, or downstream of the obstacle. Prediction of the location of the jump is beyond the scope of the present study.

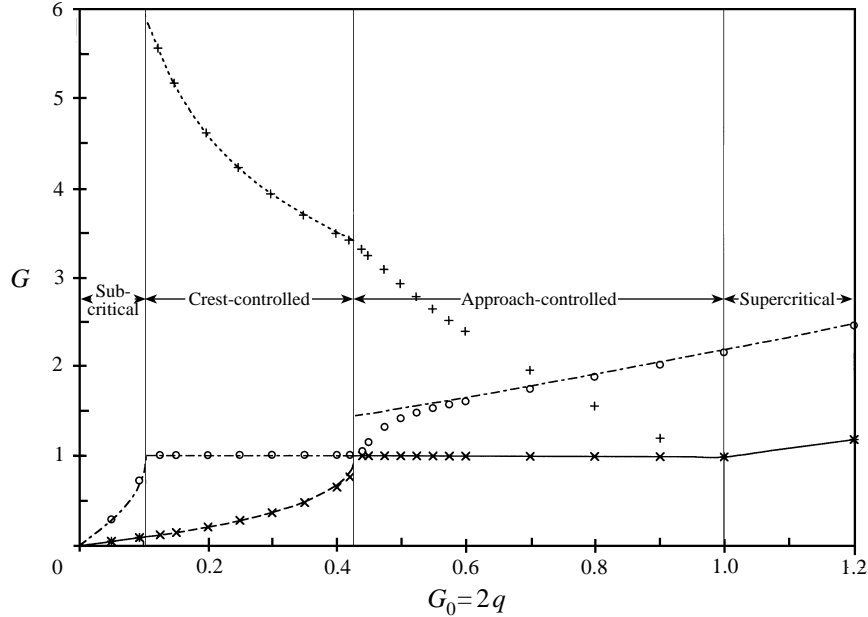


FIGURE 8. Comparisons of the predictions of the composite Froude number upstream of the obstacle, G_u , at the crest, G_c , and downstream of the obstacle, G_d , for $r = 0.5$, and $\beta_m = 0.37$. The non-hydrostatic predictions: \times , G_u ; \circ , G_c ; $+$, G_d . The hydrostatic predictions: - - - - , G_u ; - · - · - , G_c ; · · · · · , G_d . *, Identical non-hydrostatic predictions for G_u and G_d ; —, identical hydrostatic predictions for G_u and G_d .

The most substantial differences in the predictions are in Approach-controlled flows, for which hydrostatic theory predicts that the flow is symmetrical about the crest of the obstacle. Consequently, both the interface elevation and the composite Froude are the same upstream and downstream of the obstacle. On the other hand, the non-hydrostatic theory predicts a supercritical leap which results in a much lower interface elevation, and a higher composite Froude number, downstream of the obstacle. At the transition from Crest-controlled to Approach-controlled flow ($G_0 \approx 0.427$) hydrostatic theory predicts a jump in the interface elevation at the crest, whereas the inclusion of non-hydrostatic effects allows the interface elevation to rise gradually as the flow rate increases. By the time G_0 has increased to 0.55 (corresponding to the experiment modelled above) the interface elevation at the crest is only marginally less than predicted by hydrostatic theory (figure 7a). However, the interface elevation downstream of the crest is still much less than predicted by hydrostatic theory.

5. Conclusions

The assumption of hydrostatic pressure sometimes limits the applicability of hydraulic theory. We have successfully extended hydraulic theory to incorporate non-hydrostatic effects. The extended theory has been successfully applied to steady single- and two-layer shallow water flows over a smooth two-dimensional sill. While hydraulic theory gives the pressure and layer energy to accurate to $O(\sigma)$, where $\sigma = (H/L)^2 \ll 1$, the extended theory gives pressure and layer energy accurate to $O(\sigma^2)$. Unlike some other studies, the extended theory is applicable to finite size sills and to flow problems with any number of layers.

For single-layer flows, the extended theory yields the same stiff nonlinear second-

order ordinary differential equation as Naghdi & Vongsarnpigoon (1986). However, their method is not readily applicable to multi-layer flows. Naghdi & Vongsarnpigoon also failed to predict the flow owing to numerical instability. We successfully solved the equation by treating it as a boundary value problem using the approach of Ascher *et al.* (1981). The predictions of the bottom pressure and the interface position are in excellent agreement with the experimental measurements of Sivakumaran *et al.* (1983). The non-hydrostatic theory also accurately predicts the reduction in upstream depth needed to pass a given flow rate over the obstacle as a result of non-hydrostatic effects.

The extended theory was also applied to two-layer flows. It gave similar results to hydraulic theory except in the case of Approach-controlled flows. Approach-controlled flows are characterized by a supercritical leap across which the flow remains supercritical, but changes from having a thinner upper layer to having a thinner lower layer. We have shown that non-hydrostatic effects are large across a supercritical leap. Consequently, hydrostatic theory fails to model this transition, whereas the predictions of the extended non-hydrostatic theory compare well with experimental measurements.

The authors would like to thank Dr Susan Haigh for her help with mathematical derivation, Professor Uri Ascher for providing his COLNEW program, and the reviewers for their constructive comments. Financial support from the Canadian Natural Sciences and Engineering Research Council (NSERC) is gratefully acknowledged.

REFERENCES

- ARMI, L. 1986 The hydraulics of two flowing layers with different densities. *J. Fluid Mech.* **163**, 27–58.
- ARMI, L. & FARMER, D. M. 1986 Maximal two-layer exchange flow through a contraction with barotropic net flow. *J. Fluid Mech.* **164**, 27–52.
- ASCHER, U., CHRISTIANSEN, J. & RUSSELL, R. D. 1981 Collocation software for boundary-value ODEs. *ACM Trans. Math. Software* **7**(2), 209–222.
- ASCHER, U., MATTHEIJ, R. & RUSSELL, R. D. 1995 *Numerical Solution of Boundary Value Problems for Ordinary Differential Equations*. SIAM.
- BAINES, P. G. 1984 A unified description of two-layer flow over topography. *J. Fluid Mech.* **146**, 127–167.
- BAINES, P. G. 1988 A general method for determining upstream effects in stratified flow of finite depth over long two-dimensional obstacles. *J. Fluid Mech.* **188**, 1–22.
- BAINES, P. G. 1995 *Topographical Effects in Stratified Flows*. Cambridge University Press.
- BELWARD, S. R. & FORBES, L. K. 1993 Fully non-linear two layer flow over arbitrary topography. *J. Engng Maths* **27**, 419–432.
- DALZIEL, S. B. 1991 Two-layer hydraulics: a functional approach. *J. Fluid Mech.* **223**, 135.
- DRESSLER, R. F. 1978 New nonlinear shallow-flow equations with curvature. *J. Hydraul. Res.* **16**, 205–222.
- FARMER, D. M. & ARMI, L. 1986 Maximal two-layer exchange over a sill and through the combination of a sill and contraction with barotropic flow. *J. Fluid Mech.* **164**, 53–76.
- FARMER, D. M. & DENTON, R. A. 1985 Hydraulic control of flow over the sill in Observatory Inlet. *J. Geophys. Res.* **90** (C5), 9051–9068.
- HELFRICH, K. R. 1995 Time-dependent two-layer hydraulic exchange flows. *J. Phys. Oceanogr.* **25**, 359–373.
- HENDERSON, F. M. 1966 *Open Channel Flow*. Macmillan.
- KHAN, A. A. & STEFFLER, P. M. 1996 Vertically averaged and moment equations model for flow over curved beds. *J. Hydraul. Engng, ASCE* **122**, 3–9.
- KING, A. C. & BLOOR, M. I. G. 1990 Free surface flow of a stream obstructed by an arbitrary bed topography. *Q. J. Mech. Appl. Maths* **43**, 87–106.

- LAWRENCE, G. A. 1990 On the hydraulics of Boussinesq and non-Boussinesq two-layer flows. *J. Fluid Mech.* **215**, 457–480.
- LAWRENCE, G. A. 1993 The hydraulics of steady two-layer flow over a fixed obstacle. *J. Fluid Mech.* **254**, 605–633.
- LONG, R. R. 1954 Some aspects of the flow of stratified fluids. II. Experiments with a two-fluid system. *Tellus* **6**, 97–107.
- LONG, R. R. 1974 Some experimental observations of upstream disturbances in a two-fluid system. *Tellus* **26**, 313–317.
- MELVILLE, W. K. & HELFRICH, K. R. 1987 Transcritical two-layer flow over topography. *J. Fluid Mech.* **178**, 31–52.
- MURRAY, S. P., HECHT, A. & BABCOCK, A. 1983 On the mean flow in the Tiran Strait in winter. *J. Mar. Res.* **42**, 265.
- NAGHDI, P. M. & VONGSARNPIGOON, L. 1986 The downstream flow beyond an obstacle. *J. Fluid Mech.* **162**, 223–236.
- PRATT, L. J. 1984 Nonlinear flow over several obstacles. *J. Atmos. Sci.* **4**, 1212–1225.
- SHEN, S. P., SHEN, M. C. & SUN, S. M. 1989 A model equation for steady surface waves over a bump. *J. Engng Maths* **23**, 315–323.
- SHEN, S. S. 1992 Forced solitary waves and hydraulic falls in two-layer flows. *J. Fluid Mech.* **234**, 583–612.
- SIVAKUMARAN, N. S., HOSKING, R. J. & TINGSANCHALI, T. 1981 Steady shallow flow over a spillway. *J. Fluid Mech.* **111**, 411–420.
- SIVAKUMARAN, N. S., TINGSANCHALI, T. & HOSKING, R. J. 1983 Steady shallow flow over curved beds. *J. Fluid Mech.* **128**, 469–487.
- WOOD, I. R. & LAI, K. K. 1972 Flow of layered fluid over broad crested weir. *J. Hydraul. Div. ASCE* **98**, 87–104.
- ZHANG, Y. & ZHU, S. 1996 Open channel flow past a bottom obstruction. *J. Engng Maths* **30**, 487–499.
- ZHU, Z. 1996 Exchange flow through a channel with an underwater sill. PhD thesis, Dept. of Civil Engineering, University of British Columbia.